D_{2h} superlattice patterns in dielectric barrier discharge with striped water electrode*

LI Cheng[1], YAN Zhihao[1], QI Xiaoxiu[1], LI Yuxin[1], PAN Yuyang[2], DONG Lifang[1]

1.College of Physics Science and Technology, Hebei University, Baoding 071002, China

2.College of Quality and Technical Supervision, Engineering Research Center of Zero-carbon Energy Buildings and Measurement Techniques, Ministry of Education, Hebei University, Baoding 071002, China

Abstract

In this work, a special striped water electrode dielectric barrier discharge device is designed. Through numerical solutions of the Laplace equation, the spatial distribution of the applied electric field is revealed to exhibit a strip-shaped nonuniform distribution featuring the alternating regions of enhanced and weakened field intensity. These field gradients play a pivotal role in governing the plasma, for the intensified regions act as preferential sites for discharge onset, directly shaping the formation and evolution of plasma structures. Using this device, a series of novel striped patterns is observed in the discharge of a mixed gas of air and argon, marking a significant advancement in pattern formation studies. Notably, four striped superlattice patterns are obtained for the first time, each displaying intricate structural hierarchies. Among them, the large and small dot honeycomb striped superlattice pattern featuring structural complexity is chosen to investigate the formation mechanisms. The pattern is composed of three substructures: small dots, large dots, and a honeycomb framework. In the experiment, the emission spectra of different substructures are measured using a spectrograph, revealing that they are in different plasma states. The spatiotemporal dynamic behaviors of the pattern are observed using a high-speed camera and two photomultiplier tubes. It is found that the discharge sequence is small dots → large dots → honeycomb framework, where the honeycomb framework is formed by the superposition of random discharge filaments. The electric field distributions at different times are simulated by solving the Poisson equation, and the result well explains the formation mechanism of the above-mentioned patterns.

Keywords: dielectric barrier discharge, pattern, plasma

---

* The paper is an English translated version of the original Chinese paper published in Acta Physica Sinica. Please cite the paper as: **LI Cheng , YAN Zhihao, QI Xiaoxiu, LI Yuxin, PAN Yuyang, DONG Lifang, D_{2h} superlattice patterns in dielectric barrier discharge with striped water electrode.** *Acta Phys. Sin.*, 2025, 74(22): 225202.
doi: 10.7498/aps.74.20250985

PACS：52.50.Dg, 52.35.Mw, 47.54.–r, 52.80.Tn

doi: 10.7498/aps.74.20250985

cstr: 32037.14.aps.74.20250985

1. Introduction

In recent years, dielectric barrier discharge (DBD) pattern has attracted much attention as an important subject in the interdisciplinary field of plasma physics and nonlinear science[1]. Pattern, as a typical nonlinear self-organized phenomenon, has inhomogeneous structure with spatio-temporal periodicity, which widely exists in nature (such as animal surface patterns and sky cloud images),[2,3] and many experimental systems (such as Rayleigh-Benard convection system, Faraday system, chemical reaction diffusion system and dielectric barrier discharge system)[4–9]. In recent years, the pattern in dielectric barrier discharge (DBD) system has attracted much attention due to its short formation time, visible luminescence, adjustable parameters and many application prospects[10,11]. Dielectric barrier discharge (DBD) is a non-equilibrium AC gas discharge in which a dielectric is inserted into the discharge gap, also known as "silent discharge". As an interdisciplinary research hotspot of plasma physics and nonlinear science, the research results of DBD pattern not only deepen people's understanding of the self-organization behavior of complex systems, but also promote the research[12–16] of gas discharge physics, and find that it can be widely used in plasma photonic crystals, local treatment of materials and so on. Plasma photonic crystal is a periodic array of plasma and dielectric materials. Because of its dynamically tunable energy band, it has important applications in space communication and tunable microwave devices, and has attracted wide attention of researchers[17–19]. The periodic arrangement of plasma and undischarged gas in the DBD pattern is essentially a plasma photonic crystal, and the regularity and tunability of the DBD pattern make it an ideal platform for the study of plasma photonic crystals[20–22]. In addition, as a spatially ordered plasma streamer discharge mode, DBD pattern provides an effective[23–25] for material local treatment due to the high electron temperature and plasma density of the discharge filament, and different treatment effects can be achieved by adjusting the plasma parameters of the discharge filament. For example, in 2024, Dong and other[23] found that the plasma parameters can affect the etching depth and treatment efficiency by modulating the gas gap for PI film local treatment.

It is well known that the electric field distribution in dielectric barrier discharge (DBD) affects the discharge mode and current characteristics[26–29]. The analysis shows that the electric field distribution will affect the formation of dielectric barrier discharge pattern. In the past, dielectric barrier discharge (DBD) patterns were studied by using the traditional parallel plate DBD device under uniform electric field. Up to now, hexagonal pattern, square pattern, spiral

pattern and various superlattice patterns have been obtained in uniform field DBD[30–36]. In recent years, people have turned their attention to adjusting the electric field in the gas gap by designing special electrode structures, so as to explore the possibility of generating new patterns under non-uniform field conditions. In 2012, Sinclair et al.[37] used a quadrilateral needle-mesh electrode structure to introduce a wavy non-uniform electric field in the gas gap, and obtained a checkerboard pattern and a square-triangle mixed pattern. In 2016, Liu et al.[38] obtained a new type of quadrilateral superlattice pattern by attaching a very thin circular hole lattice acrylic plate with quadrilateral arrangement on the inner side of a cylindrical water electrode glass plate and introducing a lattice non-uniform electric field in the gas gap. In 2023, Chu et al.[39] introduced a square array electric field into the gas gap by pasting a very thin dielectric plate with horizontal and vertical stripes inside two cylindrical water electrodes, and obtained two kinds of quadrilateral array patterns. In general, several patterns with quadrilateral symmetry were successfully obtained by introducing a quadrilateral array electric field in the gas gap. In this work, a series of new stripe patterns with D_{2h} symmetry were obtained by designing a complete stripe water electrode DBD device, of which four kinds of D_{2h} superlattice patterns were obtained for the first time. These patterns are difficult to be obtained by the traditional parallel-plate DBD device, so this work is of great significance to promote the development of dielectric barrier discharge pattern dynamics.

In this study, a fully striped water electrode DBD device with and without water stripes distributed in an array was designed. In order to clarify its electric field control ability, the applied electric field distribution in the gas gap was calculated by solving the Laplace equation. Based on this device, many kinds of stripe patterns with D_{2h} symmetry are obtained in the discharge of air and argon mixture. The emission lines of argon atom at 696.54 nm ($2p^2 \rightarrow 1s^5$) and the second positive band system of nitrogen molecule (N_2) ($C^3\,\Pi_u \rightarrow B^3\,\Pi_g$) were collected by a spectrometer, and the electron density and vibrational temperature of different substructures in the superlattice pattern were calculated. PMT is used to measure optical signals of different substructures. Instantaneous images of frame discharge were taken by a high speed camera. The electric field distribution of large and small honeycomb superlattice patterns at different discharge time is simulated by solving Poisson equation with COMSOL Multiphysics software. In this study, the pattern of stripe array distribution is obtained by regulating the electric field, which is of great significance to promote the development of dielectric barrier discharge pattern dynamics, and also has a certain reference value to promote the regulation and application of plasma photonic crystals.

2. Experimental setup

The experimental discharge setup is shown in Fig. 1. The discharge system consists of a common water electrode and a fully striped water electrode with a distance of 2 mm. The common water electrode consists of a cylindrical transparent container with an inner diameter

of 75 mm and an outer diameter of 85 mm and a copper ring electrode, and the two ends of the container are sealed by a glass sheet with a thickness of 1.5 mm to form a flat and uniform liquid electrode surface; The fully striped water electrode is composed of a square milled groove structure and a copper ring electrode immersed in water. A rectangular groove with a width of 4 mm, a length of 70 mm and a spacing of 4 mm is machined on an acrylic plate with a length of 86 mm and a thickness of 30 mm to form a periodic stripe structure. In order to ensure the discharge synchronization in each water tank, a 10 mm wide vertical water channel is set on the right side to connect the horizontal stripes. The tank is filled with water and immersed in a copper ring, and then sealed with a 1.5 mm thick glass sheet. The copper rings of the two electrodes were connected to a 55 kHz AC power supply. A glass plate with a thickness of 2 mm was added between the electrodes, and a rectangular glass frame with a length of 40 mm and a width of 30 mm was cut on the glass as a discharge gas gap. The water electrode and the glass frame are closely attached together, and the schematic diagram is displayed separately for easy observation. The red dotted line in the Fig. 1 marks the discharge region of the fully striated electrode. The T_1 region is the position where there is water in the groove, forming a conductive channel, and the T_2 region is the position where there is no water, forming an insulating barrier. It can generate a striation array electric field corresponding to the electrode striation array in the discharge gap. The discharge device is placed in a chamber, in which the gas composition and pressure can be adjusted. The amplitudes of voltage and current were measured by a high-voltage probe (Tektronix P6015A 1000x) and a current probe (Tektronix TCP 0030a), respectively. The emission lines of argon atom at 696.54 nm ($2p^2 \rightarrow 1S^5$) and the second positive band system of nitrogen molecule ($C^3\Pi_u \rightarrow B^3\Pi_g$) were collected by a spectrometer (Acton Advanced SP 2750A, CCD: 1340 400 pixels), and a digital camera (Canon Power Shot G16) and. 120PH0047), the light from different filaments was imaged by a convex lens, and the light signals were collected by two photomultiplier tubes (PMT: RCA7265), and the waveforms were recorded by a digital oscilloscope (Tektronix TDS 4054B).

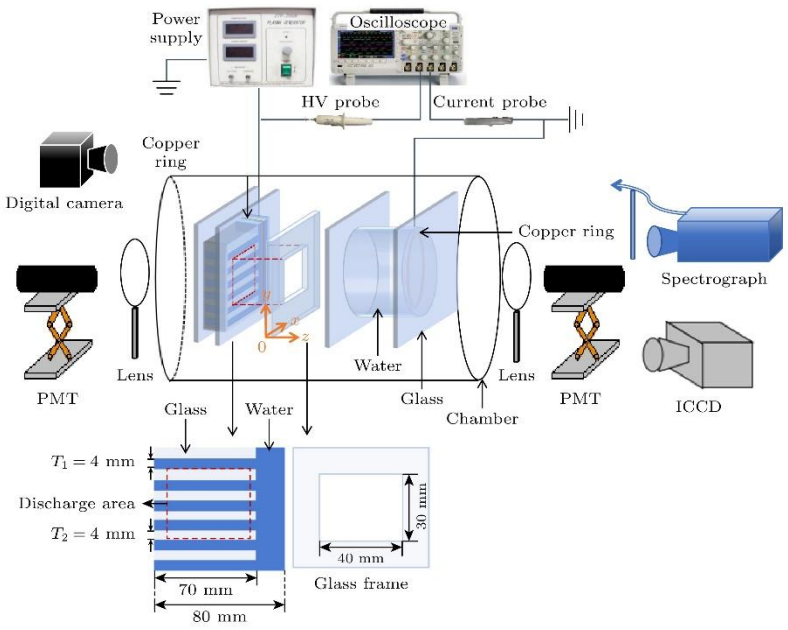

Figure 1. Schematic diagram of the experiment, T_1 region is the grooved area filled with water, while the T_2 region is the water-free area, a red dashed frame marks the discharge area on the surface of fully striped water electrode. Discharge area: length is 40 mm, width is 30 mm, gas gap d = 2 mm.

Fig. 2 is the electric field distribution map of the *x*-*y* plane at different *z* positions, in which the T_1 region (the position where there is water in the groove) is marked in blue, and the T_2 region (the position where there is no water) is marked with diagonal stripes. If the three-dimensional coordinate system is established by Fig. 1, the zero point is set on the surface of the completely striped water electrode in the gas gap (marked by the orange arrow), and the direction pointing to the ordinary water electrode is the positive direction of the *z* axis. The simulated electric fields at the cross sections of z = 0 mm, z = 1 mm and z = 2 mm are taken respectively, and the simulated voltage of the external field is U = 2.5 kV. From the simulation results, it can be seen that the electric field intensity in the T_1 region of the modulated water electrode is greater than that in the T_2 region, so the non-uniform electric field of the stripe array is generated in the gas gap.

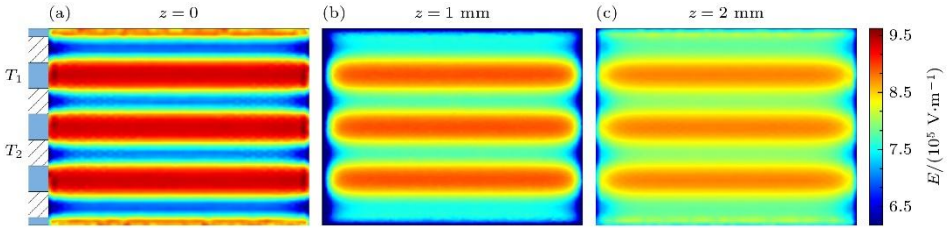

Figure 2. Spatial distribution of applied electric field in the gas gap: (a)–(c) Electric field distribution in *x*-*y* plane at different *z* values, the applied voltage is 2.5 kV.

3. Experimental results and discussion

3.1 Stripe pattern Obtained by Complete Fringe Water Electrode DBD Device

By adjusting the χ of argon content and the p of gas pressure in the complete striped water electrode device, a variety of new striped patterns were obtained, as shown in the Fig. 3. In air with p = 10 kPa, when the voltage reaches the breakdown threshold U = 2.2 kV, the discharge only occurs in the region of T_1, forming a stripe pattern, as shown in Fig. 3(a), which is consistent with the electric field simulation results of Fig. 2. When the voltage is increased to U = 2.8 kV, the discharge in the T_1 region becomes a large dot, and a halo discharge also appears in the T_2 region, forming a stripe superlattice pattern composed of a large dot and a halo, as shown in Fig. 3(b). As the voltage is further increased to U = 3.2 kV, the large dots in the T_1 region become small dots with smaller spacing, and the halo discharge in the T_2 region becomes large dots, forming a large and small dot stripe superlattice pattern, as shown in Fig. 3(c). By adjusting the pressure, the double stripe pattern containing the halo is obtained, as shown in Fig. 3(d). The discharge gas is a mixture of air and argon, and the large and small honeycomb superlattice pattern is obtained, as shown in Fig. 3(e). The honeycomb superlattice pattern is obtained by increasing the voltage, as shown in Fig. 3(f). It is worth pointing out that the superlattice patterns in Fig. 3(b),(c),(e) and(f) are found for the first time in DBD systems.

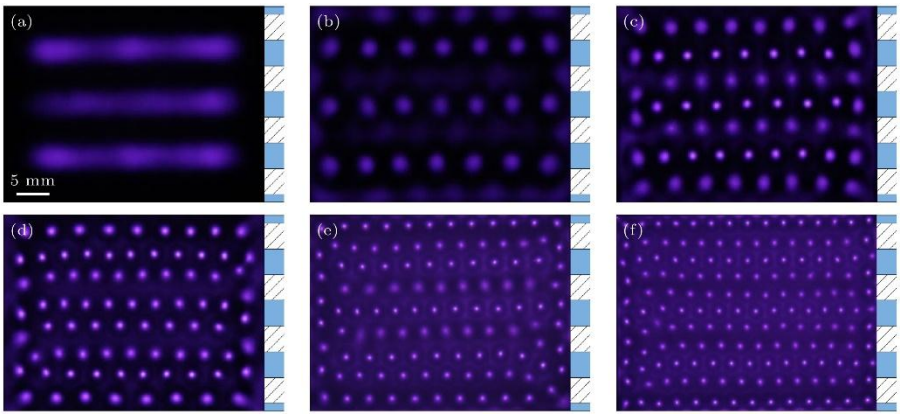

Figure 3. Stripe patterns under different discharge parameters (argon content χ in air-argon mixture, pressure p, voltage U): (a) Stripe pattern, χ = 0, p = 10 kPa, U = 2.2 kV; (b) large dot halo stripe pattern, χ = 0, p = 10 kPa, U = 2.8 kV; (c) large and small dots stripe superlattice pattern, χ = 0, p = 10 kPa, U = 3.2 kV; (d) double stripe pattern, χ = 0, p = 15 kPa, U = 3.8 kV; (e) large and small dots honeycomb stripe superlattice pattern, χ = 30%, p = 20 kPa, U = 4.4 kV; (f) stripe honeycomb superlattice pattern, χ = 30%, p = 20 kPa, U = 4.8 kV.

In the isotropic uniform electric field of the traditional DBD device, the quadrilateral, hexagonal and spiral patterns are more common. As mentioned above, in the study of

modulated electrodes in recent years, most of the lattice patterns with quadrilateral symmetry have been obtained. In this work, a variety of stripe array patterns with D_{2h} symmetry can be obtained in a completely striped water electrode, which enriches the pattern types and is of great significance to the development of dielectric barrier discharge pattern dynamics.

3.2 A study of large and small point honeycomb fringe superlattice spot pattern

3.2.1 Evolution sequence and phase diagram

In order to understand the formation mechanism of the stripe pattern generated in the fringe electrode, the Fig. 3(e) (honeycomb fringe superlattice pattern) with the most complex structure is selected for study. The Fig. 4 is the evolution sequence of pattern type with the increase of applied voltage, and other discharge conditions are p = 20 kPa and χ = 30%. When the voltage reaches the breakdown threshold U = 2.8 kV, the discharge filaments are preferentially generated in the T_1 region and present a strip array arrangement, resulting in an initial pattern, as shown in the Fig. 4(a). As the voltage increases to U = 3.4 kV, the discharge filaments in the T_1 region become smaller, and there are also discharge filaments in the T_2 region, as shown in Fig. 4(b), forming a double stripe pattern containing halos. As the voltage is further increased to U = 4.4 kV, a honeycomb frame appears around the discharge filament in the T_1 region, and a large and small point honeycomb fringe superlattice pattern of the honeycomb frame with fringe arrangement is formed through self-organization, as shown in Fig. 4(c). When the voltage U = 4.8 kV, the discharge filaments are more closely arranged and the honeycomb frame still exists, as shown in Fig. 4(d).

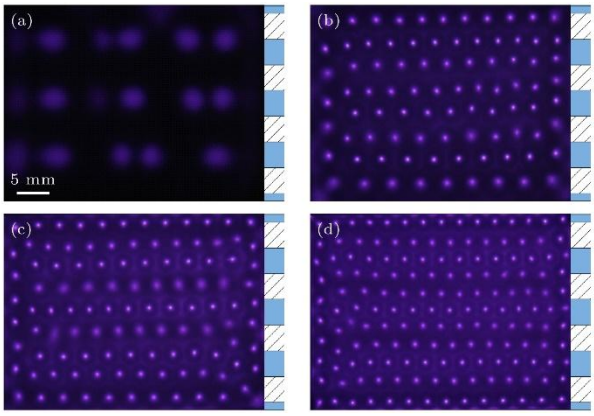

Figure 4. Evolution sequence of large and small dots honeycomb stripe superlattice pattern with voltage increase: (a) Initial pattern, U = 2.8 kV; (b) double stripe pattern, U = 3.4 kV; (c) large and small dots honeycomb stripe superlattice pattern, U = 4.4 kV; (d) stripe honeycomb superlattice pattern, U = 4.8 kV, other experimental parameters: p = 20 kPa, χ = 30%.

In order to intuitively show the difference and ratio of the brightness of different substructures of the honeycomb fringe superlattice pattern, the Fig. 5 shows the light intensity distribution

of the discharge filament at different positions. The large and small dot honeycomb stripe superlattice pattern is composed of small dots (S), honeycomb frames (F) and large dots (L), wherein the small dots and the honeycomb frames are in T_1 region, and the large dots are in T_2 region, as shown in the Fig. 5(a). The light intensity distribution in the white frame in the Fig. 5(a) is calculated by Matlab, and the light intensity distribution is shown in the Fig. 5(b). It is found that the brightness of the small dot, the large dot and the honeycomb frame is 237, 129 and 60, respectively, and the brightness ratio of the three is about 4 ∶ 2 ∶ 1.

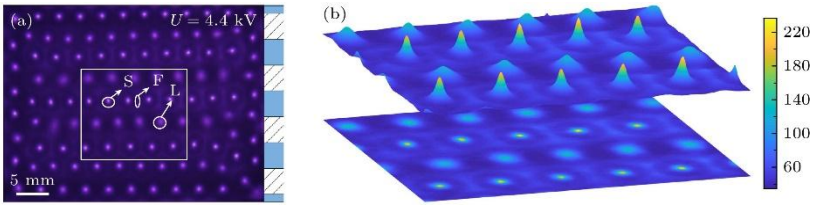

Figure 5. Light intensity distribution of the large and small dots honeycomb stripe superlattice pattern: (a) Photograph of the large and small dots stripe superlattice pattern, the white border outlines the simulated light intensity area; (b) light intensity distribution of the pattern.

It is found that the formation of large and small honeycomb superlattice patterns is related to gas pressure, gas composition and applied voltage. The Fig. 6 is the phase diagram of the pattern evolution and the large and small point honeycomb superlattice pattern. It can be seen that when the χ is 0 — 50%, the U is 2.4 — 5.9 kV, and the p is in the range of 8 — 28 kPa, the large and small honeycomb superlattice patterns can be observed.

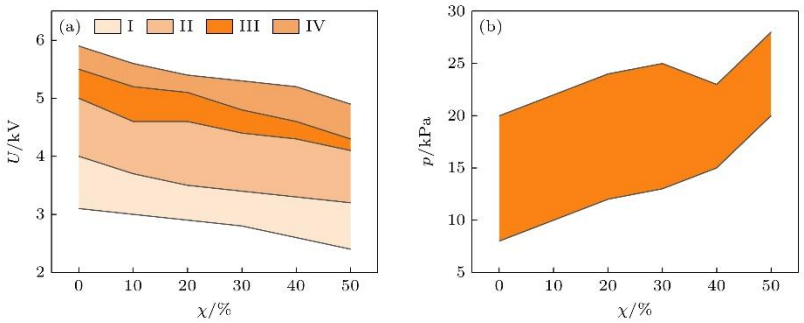

Figure 6. (a) Phase diagram of the evolution process of the large and small dots honeycomb stripe superlattice pattern as a function of the voltage U and the argon content χ; (b) phase diagram of the large and small dots honeycomb stripe superlattice pattern as a function of the gas pressure p and argon content χ.

3.2.2 Spectroscopic diagnosis of plasma parameters

In order to explore the plasma States of different substructures, the Ar I (696.54 nm, $2p^2 \rightarrow 1s^5$) lines and the nitrogen second positive band system ($C^3\Pi_u \rightarrow B^3\Pi_g$) of different substructures were collected by spectrometer, and the electron density and vibrational temperature were calculated.

The Fig. 7(a) gives the Ar I lines of S, L and F. The Stark broadening method was used to estimate the electron density[40–42], and the results are shown in Fig. 7(b). The electron densities of substructures S, L and F are $(6.0 \pm 0.7) \times 10^{15}$, $(5.4 \pm 0.9) \times 10^{15}$ and $(7.0 \pm 1.0) \times 10^{15}$ cm^{-3}, respectively. Therefore, the three substructures have different electron densities, with the lowest electron density of large dot L and the highest electron density of honeycomb frame F. The emission lines of the second positive band system of nitrogen molecule ($C^3\Pi_u \rightarrow B^3\Pi_g$) with different substructures are shown in Fig. 7(c). The vibrational temperatures were estimated[43] by using two groups of vibrational bands of the second positive band system: $\Delta v = -2$ (0 – 2, 1 – 3, 2 – 4) and $\Delta v = -3$ (0 – 3, 1 – 4, 2 – 5). The calculation results are shown in Fig. 7(d). The molecular vibrational temperatures of S, L and F are (3000 ± 50) K, (3010 ± 50) K and (3760 ± 50) K. It is obvious that the molecular vibrational temperatures of S and L.

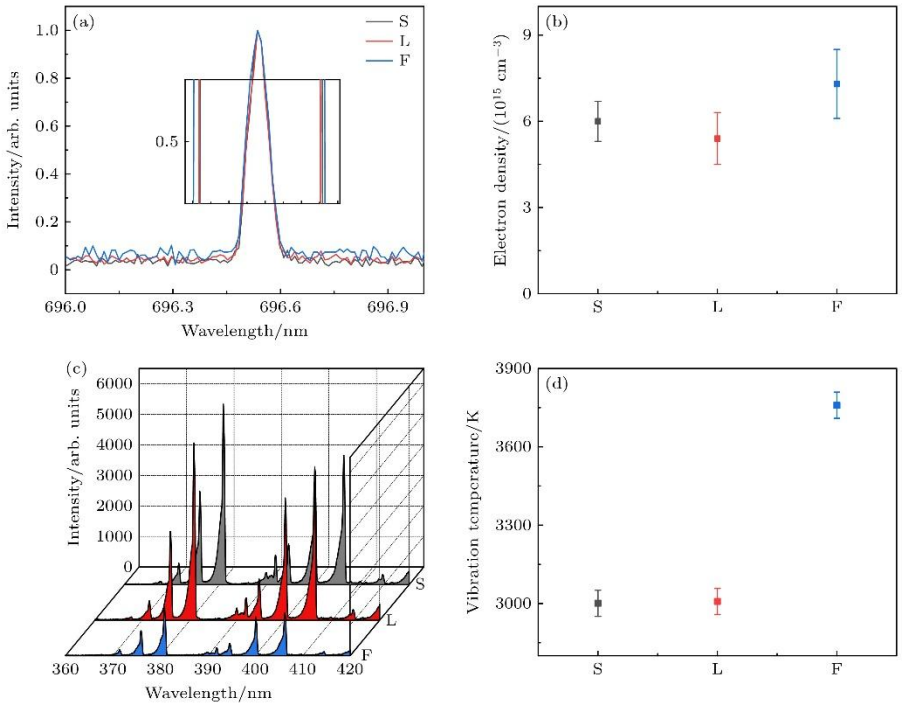

Figure 7. Emission spectra of the large and small dots honeycomb stripe superlattice pattern: (a) Spectral line at 696.54 nm and magnified central region for different substructures; (b) electron density values for substructures S, L and F; (c) N_2 emission spectra of substructures

within 360–420 nm; (d) vibrational temperatures for substructures S, L and F.

To sum up, the electron density and molecular vibrational temperature of the three substructures are significantly different, indicating that they are in different plasma States. Furthermore, after comparing the distribution characteristics of electron density and molecular vibrational temperature with the distribution of applied electric field shown by Fig. 2, it is found that the spatial distribution of plasma parameters is not completely consistent with the distribution of applied electric field. For example, the electron density of S and F is larger than that of L in the T_1 region where the external electric field is larger, and the electron density of S and F is larger than that of L in the T_2 region where the external electric field is weaker, which is consistent with the electric field distribution. However, the vibration temperatures of S and L are basically the same, but both are lower than that of F, which indicates that the discharge behavior of the pattern is not only regulated by the applied electric field, but also closely related to the self-organization process of the discharge filament. In order to reveal the discharge mechanism of the pattern, we used a photomultiplier tube and a high-speed camera to further measure its spatiotemporal dynamic characteristics.

3.2.3 Spatiotemporal dynamics measurement

The time correlation of different substructures measured by photomultiplier tube is given in Fig. 8 to study the formation mechanism of large and small honeycomb superlattice patterns. The Fig. 8(a) shows a photograph of the pattern, where S and F are located in the T_1 region of the modulated water electrode and L is located in the T_2 region of the modulated water electrode. The Fig. 8(b) shows the current-voltage waveform of the positive half cycle. It can be found that the current waveform is composed of three parts, and the pulse width is represented by Δt_1, Δt_2, Δt_3, respectively. Fig. 8(c) shows the spatiotemporal correlation of the optical signals of S and L. It is found that S discharges earlier than L, and S corresponds to the first pulse and L corresponds to the second pulse. The superposition of S and F optical signals is given by Fig. 8(d), and it is found that F corresponds to the subsequent continuous pulse. To sum up, the optical signals of S, L and F correspond to the first, second and subsequent pulses of the current pulse respectively, and these three optical signals are distributed to discharge at the rising edge of the voltage, so the discharge sequence of the large and small point honeycomb fringe superlattice pattern is S → L → F.

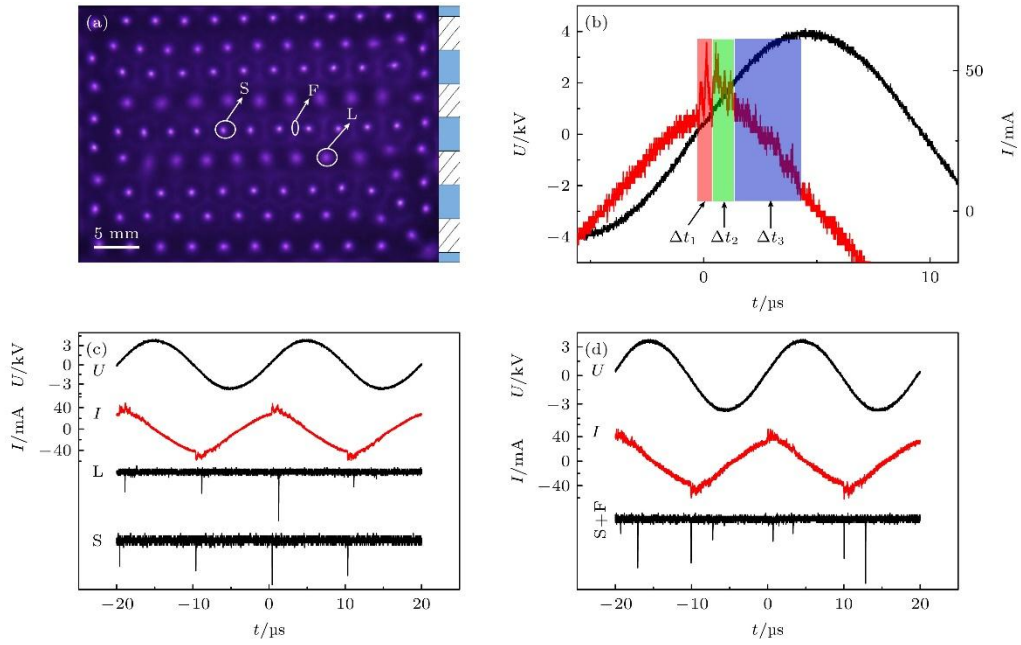

Figure 8. Spatial-temporal structure dynamics measurement of large and small honeycomb stripe superlattice pattern: (a) Image of the pattern; (b) waveforms of voltage and current of the pattern in the positive half-cycle; (c) temporal correlation measurement of S and L; (d) temporal correlation measurement of S and F.

In order to reveal the formation mechanism of the fringe array honeycomb frame, the third current pulse of Fig. 8(b) (exposure time Δt_3) was photographed by a high-speed camera with different superimposed periods, as shown in the Fig. 9. The Fig. 9(a) —(d) shows the discharge images with 1, 20, 50 and 100 superposition cycles, respectively. The experimental results show that when the superposition period is 1, the image only shows discrete random discharge filaments, and the honeycomb structure cannot be identified; As the number of superposition increases to 20, the discharge filaments gather in a specific area and begin to show the rudiment of the honeycomb frame; When the superposition period reaches 50 times, the periodicity of the honeycomb frame is significantly enhanced. Finally, after 100 times of superposition, the honeycomb frame presents a highly ordered hexagonal stripe structure. By comparing these pictures, it is shown that although the honeycomb frame appears as a continuous luminous band macroscopically, its microcosmic composition is still random discharge filaments.

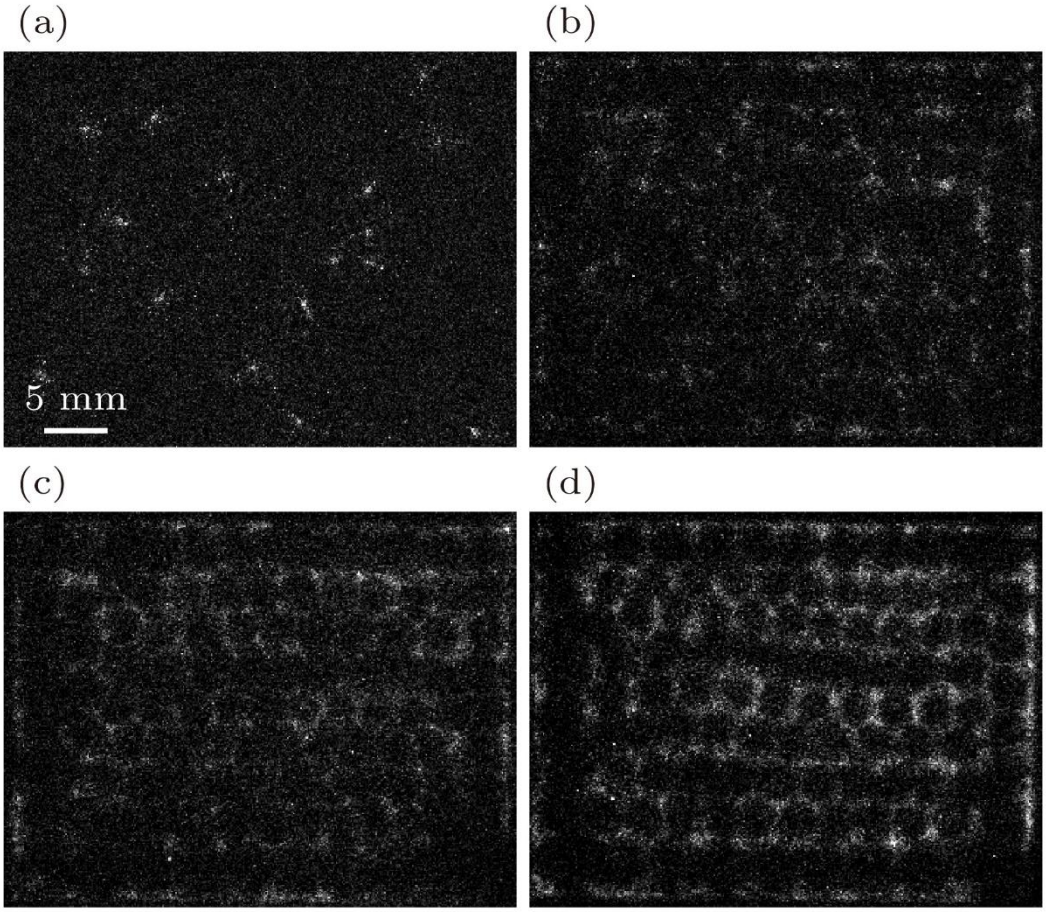

Figure 9. Photos of the frame superimposed with different voltage periods. At an exposure time of Δt_3: (a)–(d) Correspond respectively to the photographs with superimposed voltage cycles of 1, 20, 50, and 100.

To sum up, using photomultiplier tube and high-speed camera, it is found that the discharge sequence is small spot → large spot → honeycomb frame, and the honeycomb frame is composed of random discharge filaments. It is worth pointing out that the large dot in the T_2 region discharges earlier than the honeycomb frame in the T_1 region, which indicates that the discharge of the pattern is not only related to the applied electric field distribution, but also a self-organization process involving wall charges. Therefore, it is necessary to solve the Poisson equation with wall charge to further analyze the discharge mechanism.

3.2.4 Spatiotemporal evolution of electric field

The electric field formed after discharge at different times is simulated by solving the Poisson equation with COMSOL software, and the space-time evolution results of the electric field are given as Fig. 10.

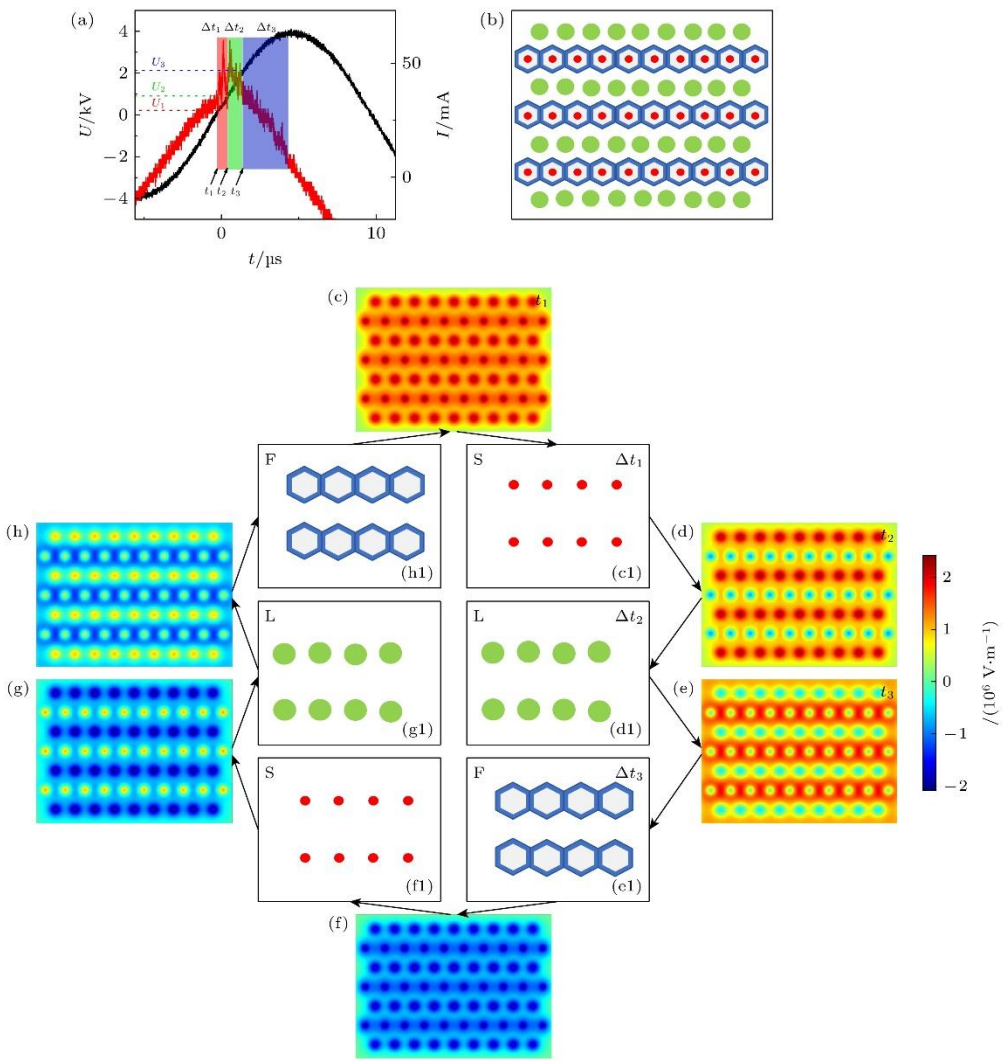

Figure 10. Electric field distributions at different moments of the large and small dot honeycomb stripe superlattice pattern and the corresponding schematic diagrams of substructure: (a) Applied voltage and current waveforms for the pattern; (b) schematic diagram of the pattern; (c)–(e) electric field distributions in the gas gap at t_1, t_2, and t_3 during the positive half-cycle; (f)–(h) correspond respectively to the electric field distributions before the discharge of each substructure in the negative half-cycle; (c1)–(h1) schematic illustrations of substructure discharge corresponding to the electric fields in panels (c)–(h).

Poisson equation:

$$\nabla^2\psi = -\rho/(\varepsilon_r\varepsilon_0), \tag{1}$$

Where ψ stands for electric potential, ρ stands for charge density, ε_r stands for dielectric constant of medium, and ε_0 stands for dielectric constant of vacuum. The relationship between electric field and electric potential of space is given by the following formula:

$$\boldsymbol{E} = -\nabla\psi. \tag{2}$$

For the calculation of ρ, it is first calculated by integrating the current pulses corresponding to S, F and L:

$$Q = \int_{t_2}^{t_1} I\mathrm{d}t, \tag{3}$$

The amount of wall charge accumulated after S, F, L discharge was obtained as Q_S = 6.93 × 10^{-9} C, Q_F = 4.94 × 10^{-9} C, and Q_L = 1.28 × 10^{-8} C. Then according to the formula:

$$\rho = \frac{Q}{nS}, \tag{4}$$

Where n is the number of discharge filaments and S is the area of discharge filaments, the charge surface density of different substructures is obtained as ρ_S = 2.94 × 10^{-4} C/m^2, ρ_F = 3.15 × 10^{-5} C/m^2, and ρ_L = 1.02 × 10^{-4} C/m^2. It is worth pointing out that the charge surface density distribution is consistent with the light intensity distribution of Fig. 5.

Fig. 10 gives the variation of the electric field and discharge with time in an applied voltage cycle. Fig. 10(a) shows the voltage and current waveforms of the pattern.t_1,t_2,t_3 are recorded as the start time of Δt_1, Δt_2, Δt_3 in Fig. 8(b), respectively, and the corresponding discharge voltage is given. Fig. 10(b) is the schematic diagram of the structure of the pattern. The small dot, the large dot and the honeycomb frame are represented by the small red circle, the large green circle and the blue regular hexagon, respectively. Fig. 10(c) —(e) is the electric field distribution of t_1, t_2 and t_3 in the gas gap. Schematic diagram of substructure discharge in the period of Δt_1, Δt_2 and Δt_3 from Fig. 10(c1) to(e1), respectively. It can be seen from Fig. 10(c) (U_1 = 0.3 kV, t =t_1) that the field strength at the position of the small dot is the largest, and Δt_1 corresponds to the small dot discharge structure of the strip array distribution, such as Fig. 10(c1). The electric field distribution after the small spot discharge is shown as Fig. 10(d) (U_2 = 0.9 kV, t =t_2). It can be seen that the field strength at the position of the large spot is the largest. With the increase of the voltage, Δt_2, there is also a large spot discharge in the strip array arrangement, as shown in Fig. 10(d1). The electric field distribution after large spot discharge is Fig. 10(e) (U_3 = 2.1 kV, t =t_3), and the field strength at the honeycomb frame is the largest, so the next discharge structure is the honeycomb frame such as Fig. 10(e1). Due to

the forbidden effect of the wall charge at the position of the small spot, the discharge filaments are generated in the area far away from the small spot, and finally the honeycomb frame with strip array arrangement is formed. When the applied voltage changes polarity, the above process will be repeated. In the negative half period, the electric field distribution and the discharge substructure in the gap at the beginning of the discharge of the three substructures are shown as Fig. 10(f) —(h) and Fig. 10(f1) —(h1), respectively.

From the results of the spatio-temporal evolution of the electric field and discharge in the Fig. 10, it can be seen that there is a significant interaction between the electric field and discharge: the distribution of the electric field determines the location of the discharge, and the wall charge accumulated by the discharge will affect the distribution of the electrical field at the next moment, and so on, and finally form a stable pattern through self-organization.

In the fully striped water electrode discharge device, the electric field of the stripe array is coupled with the self-organization process of the discharge, and then various types of stripe array patterns are obtained, which provides a help for the study of pattern dynamics; These stripe patterns are essentially plasma photonic crystals with periodic arrangement of plasma and undischarged gas. Compared with traditional photonic crystals with fixed band structure, plasma photonic crystals have tunable flexibility. In recent years, stripe patterns have attracted much attention because of their unique one-dimensional periodic structure[19,44–46]. In 2014, Zhang et al. Obtained a one-dimensional plasma photonic crystal[19] through a discharge tube with stripe distribution. In 2021, Polonskyi et al.[46] obtained a striped DBD pattern that can be used for local treatment of materials by introducing an acrylic plate with a striped pattern in the discharge gap. The above studies show that the stripe pattern plays an important role in the fields of plasma photonic crystals and local processing of materials. Various stripe patterns can be obtained by adjusting the discharge parameters in this device, which provides a new scheme for the study of plasma photonic crystals and an effective method for the local treatment of materials in DBD systems.

4. Conclusion

In this work, a fully striated water electrode dielectric barrier discharge (DBD) device was designed to generate striated array electric field. In order to explore its electric field control ability, the applied electric field in the gas gap is calculated by solving the Laplace equation, and it is found that the electric field presents a stripe-like non-uniform electric field distribution, and the electric field intensity in the T_1 region with water is significantly higher than that in the T_2 region without water. Discharge through a mixture of air and argon. Many new types of stripe patterns with D_{2h} symmetry have been observed in this device, among which four kinds of fringe superlattice patterns are obtained for the first time, and the most complex large and small point honeycomb fringe superlattice patterns are studied. The pattern is composed of three sets of discharge filament structures: small dot, large dot and

honeycomb frame. The emission spectra of Ar I (696.54 nm, $2p^2 \rightarrow 1s^5$) and the second positive band system of nitrogen molecule (N_2) ($C^3\,\Pi_u \rightarrow B^3\,\Pi_g$) with different substructures were collected by spectrometer, and the electron density and vibrational temperature were calculated. It was found that different substructures were in different plasma States. Through the study of the spatiotemporal structure dynamics of the photomultiplier tube and the honeycomb fringe superlattice pattern of large and small dots, it is clear that the discharge sequence is small dot → large dot → honeycomb frame. The honeycomb frame was photographed by a high-speed camera at different time scales, and the results show that the microstructure of the honeycomb frame is composed of random discharge filaments.

The electric field distribution at different discharge time is obtained by solving the Poisson equation with COMSOL software, and the spatio-temporal evolution of the electric field is obtained. The results show that the fully striped water electrode makes the substructure of the pattern present the strip distribution characteristics, and the substructure of the previous discharge will affect the next discharge process, and finally the striped array pattern is formed, which well explains the experimental phenomenon. In this study, the pattern of D_{2h} stripe array distribution is obtained by controlling the electric field, which promotes the development of pattern dynamics and provides a new scheme for the band gap control of plasma photonic crystals.

References

[1] Kogelschatz U 2010 J. Phys. Conf. Ser. 257 012015

[2] Joron M, Jiggins C D, Papanicolaou A, McMillan W O 2006 Heredity 97 157

[3] Werner T, Koshikawa S, Williams T M, Carroll S B 2010 Nature 464 1143

[4] Rogers J L, Schatz M F, Brausch O, Pesch W 2000 Phys. Rev. Lett. 85 4281

[5] Perkins A C, Grigoriev R O, Schatz M F 2011 Phys. Rev. Lett. 107 064501

[6] Cominotti R, Berti A, Farolfi A, Zenesini A, Lamporesi G, Carusotto I, Recati A, Ferrari G 2022 Phys. Rev. Lett. 128 210401

[7] Frumkin V, Gokhale S 2023 Phy. Rev. E 108 L012601

[8] Bánsági T, Vanag V K, Epstein I R 2011 Science 331 1309

[9] Kameke A V, Huhn F, Mu ñuzuri A P, Mu ñuzuri V P 2013 Phys. Rev. Lett. 110 088302

[10] Dong L F, He Y F, Yin Z Q, Chai Z F 2004 Plasma Sources Sci. Technol. 13 164.

[11] Guikema J, Miller N, Niehof J, Klein M, Walhout M 2000 Phys. Rev. Lett. 85 3817

[12] Zhang B, Zhang X B, Wu S Q 2024 J. Appl. Phys. 136 203304

[13] Peng B F, Wang R Z, Li J, Jiang N, Yuan D K, Chen Z Q, Lei Z P, Kang A L, Song J C 2024 Appl. Phys. Lett. 125 144102

[14] Peng B F, Jiang N, Zhu Y F, Li J, Wu Y 2024 Plasma Sources Sci. Technol. 33 045018

[15] Peng B F, Li J, Jiang N, Jiang Y, Chen Z Q, Lei Z P, Song J C 2024 Phys. Fluids 36 037144

[16] Liu Q J, You M, Wang J M, Chen Y Y, Guo Z H, Zhu S S, Wu S Q 2024 IEEE Trans. Plasma Sci. 52 3166

[17] Li J F, Yao J F, Wang Ying, Zhou Z X, Lan Z H, Yuan C X 2024 Adv. Opt. Mater. 12 2303244

[18] Wang R G, Li B, Zhang T K, Ouyang J T, Sun Y R 2020 Plasma Sci. Technol. 22 085002

[19] Zhang L, Ouyang J T 2014 Phys. Plasmas 21 103514

[20] Liu F C, Liu Y N, Liu Q, Wu Z C, Liu Y H, Gao K Y, He Y F, Fan W L, Dong L F 2022 Plasma Sources Sci. Technol. 31 025015

[21] Dong L F, Li Y H, Yan Z H, He Y N, Li C, Pan Y Y 2025 Chaos Soliton Fractals 200 117023

[22] Dong L F, Li Y H, Qi X X, Fan W L, Li R, Liu S, Pan Y Y 2025 Opt. Express 33 37246

[23] Dong L F, Zhang L J, He Y N, Wei T, Li Y H, Li C, Pan Y Y 2024 Appl. Phys. Lett. 125 104101

[24] Ongrak P, Poolyarat N, Suksaengpanomrung S, Saidarasamoot K, Jirakiattikul Y, Rithichai P 2023 Horticulturae 9 1269

[25] Kim S J, Kim S, Son B K, Lee K H, Park B J, Cho G 2020 J. Korean Phys. Soc. 77 572

[26] Fan W L, Hou X H, Tian M, Gao K Y, He Y F, Yang Y X, Liu Q, Yao J F, Liu F C, Yuan C X 2022 Plasma Sci. Technol. 24 015402

[27] Yao J X, Miao J S, Li J X, Lian X Y, Ouyang J T 2023 Appl. Phys. Lett. 122 082905

[28] Ouyang J T, Duan X X, Xu S W, He F 2012 Chin. Phys. Lett. 29 025201

[29] Duan X X, Ouyang J T, Zhao X F, He F 2009 Phys. Rev. E 80 016202

[30] Dong L F, Xiao H, Fan W L, Zhao H T, Yue H 2010 IEEE Trans. Plasma Sci. 38 2486

[31] Dong L F, Li B, Lu N, Li X C, Shen Z K 2012 Phys. Plasmas 19 052304

[32] Dong L F, Li B, Shen Z K, Wang Y J, Lu N 2012 Phys. Rev. E 86 036211

[33] Dong L F, Liu B B, Li C X, Pan Y Y 2019 Phys. Rev. E 100 063201

[34] Dong L F, Liu W B, Wang Y J, Zhang X P 2014 IEEE Trans. Plasma Sci. 42 2

[35] Li C X, Feng J Y, Wang S C, Li C, Ran J X, Pan Y Y, Dong L F 2024 Plasma Sci. Technol. 26 085401

[36] Dong L F, Mi Y L, Pan Y Y 2020 Phys. Plasmas 27 023504

[37] Sinclair J, Walhout M 2012 Phys. Rev. Lett. 108 035005

[38] Liu W B, Wang Y J, Zhang H, Pan Y Y, Dong L F 2016 Rev. Sci. Instrum. 87 056101

[39] Chu J H, Dong L F, Tian M, Li Y H, He Y N, Zhang J H, Pan Y Y 2024 Sci. China-Phys. Mech. Astron. 54 245212

[40] Dong L F, Qi Y Y, Liu W Y, Fan W L 2009 J. Appl. Phys. 106 013301

[41] Dong L F, Qi Y Y, Zhao Z C, Li Y H 2008 Plasma Sources Sci. Technol. 17 015015

[42] Dong L F, Ran J X, Mao Z G 2005 Appl. Phys. Lett. 86 161501

[43] Li Y H, Pan Y Y, Tian M, Wang Y, He Y N, Zhang J H, Chu J H, Dong L F 2023 Phys. Plasmas 30 033502

[44] Feng J Y, Pan Y Y, Li C X, Liu B B, Dong L F 2020 Phys. Plasmas 27 063516

[45] Wang Y F, Wang L, Guo D, Fan X L, Harati J, Huang H, Chen P F, Chen X G, Guo T L, Weng J, Deng K 2025 Chem. Eng. Sci. 311 121537

[46] Polonskyi O, Hartig T, Uzarski J R, Gordon M J 2021 Appl. Phys. Lett. 119 211601